Synthetic aperture radar data processing

Rick Ottolini

ABSTRACT

Synthetic aperture radar (SAR) data is imaged similar to Vibroseis seismic data. There is a correlation-deconvolution stage and a migration stage. Differences include a very large aperture, an acquisition slant correction, careful attention to aliasing, and complex modulus display of specular images.

INTRODUCTION

Comparative research between seismic and SAR imaging synergistically benefits both areas. Rocca (1987) describes the principles of both methods. This paper takes an operational point of view.

Table 1 compares and contrasts seismic and SAR data processing. It is mainly derived from Rocca (1987).

Comparison Table

SEISMIC	SAR
Geometry	
time	range
midpoint	azimuth
dip	source-receiver doppler motion
linear moveout	squint angle
cross dips	terrain elevation
Acquisition	
acoustic	electromagnetic
Vibroseis sweep	chirp wavelet
low-pass	bandpass

10-50 Hz	1.331 ±.02 GHz
non-zero offsets	zero offset (current)
50m CDP	5m CDP
λ=50m $\geq$ CDP	λ = .2m << CDP
speckle	none
thousands of midpoints	16K channels
thousands of time samples	14K time samples
Processing	
source deconvolution	source correlation
migration	azimuth deconvolution
variable media velocity	$\simeq$ constant velocity (light)
100s midpoint diffractions	10000s channel diffractions
non-coherent stack	multiple 'looks'
wavefield display	modulus display

PROCESSING SEQUENCE

Figure 1 outlines the processing sequence. It resembles Vibroseis data processing. The dataset used in this article is from the toe-of-Italy region.

Correlation

Correlation to compresses the source chirp wavelet (Figures 2-4). The wavelet duration (1500 samples; Figure 4) is 11% of the record length (13860 samples). The ends of the record may contain an interesting part of the image, so it is important to avoid correlation-end artifacts.

Spatial deconvolution

The correlated data (Figure 4) contain azimuthal streaks analogous to diffraction hyperbolas on reflection seismograms. The diffraction aperture is huge, spanning many thousands of channels. Spatial deconvolution (migration) collapses the streaks. Frequency-domain spatial deconvolution is computationally more efficient than azimuthal summation methods (Kirchoff migration). In addition, image enhancement techniques described later use sub-bands of the frequency range.

The imaging transfer function contains both phase shift (Gazdag, 1978) and interpolation (Stolt, 1978) components:

$$U(k_x, k_\tau) = U\left(k_x, \sqrt{k_\tau^2 + \frac{k_x^2 c^2}{4}}\right) e^{-i\sqrt{k_\tau^2 + \frac{k_x^2 c^2}{4}}\tau_0 + ik_\tau \tau_0}, \qquad (1)$$

where k_x, ω, and k_τ are the range, azimuthal, and image-range wavenumbers and obey the dispersion relation

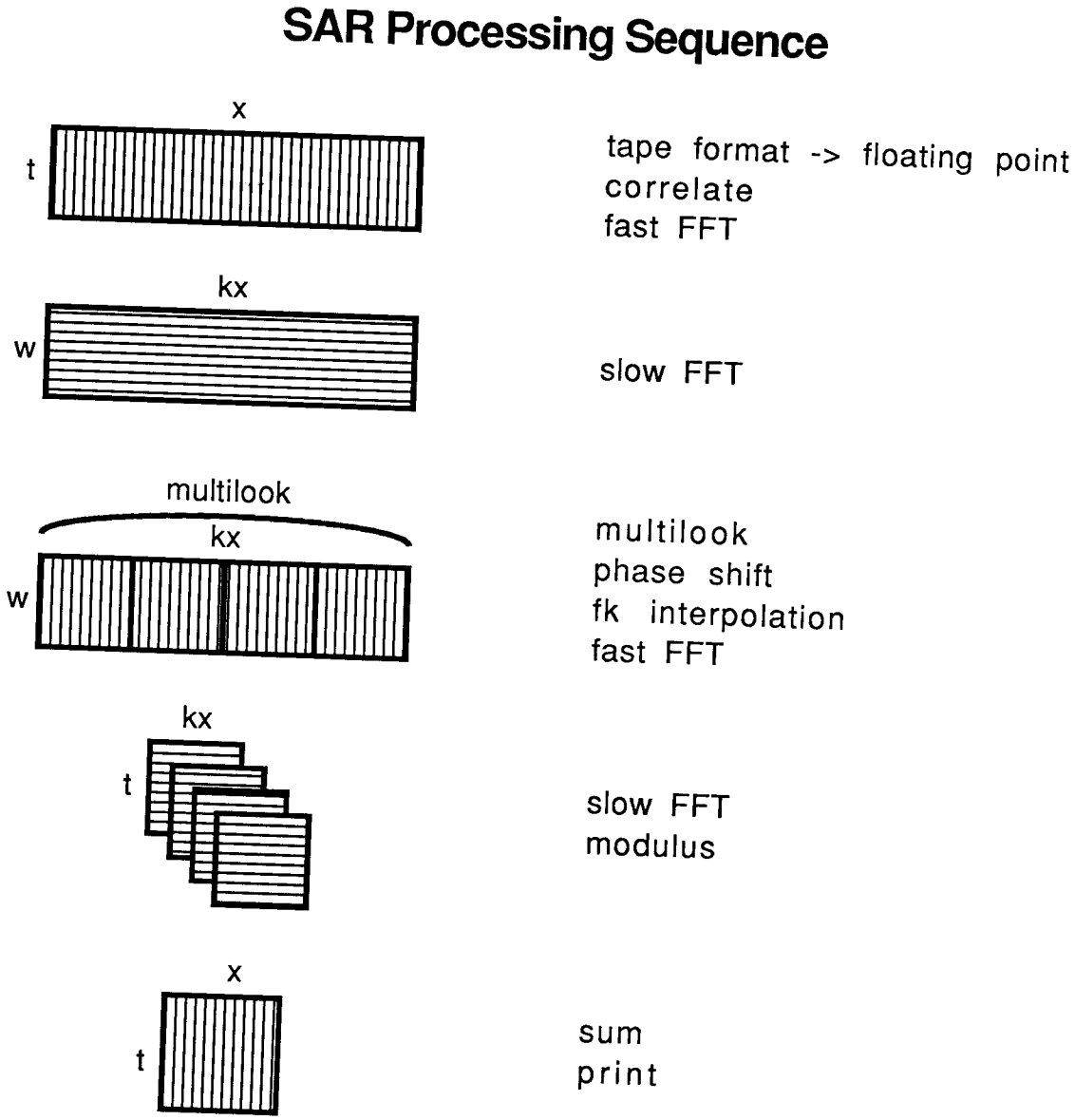

FIG. 1. SAR data processing sequence.

$$\omega^2 = k_\tau^2 + \frac{k_x^2 c^2}{4}. \tag{2}$$

c is the velocity of the radar, and τ_0 the delay of the radar signal to the earth and back. The root term in equation (1) accounts for the azimuthal motion of the radar source-receiver. The $k_\tau \tau_0$ term is the time delay phase shift.

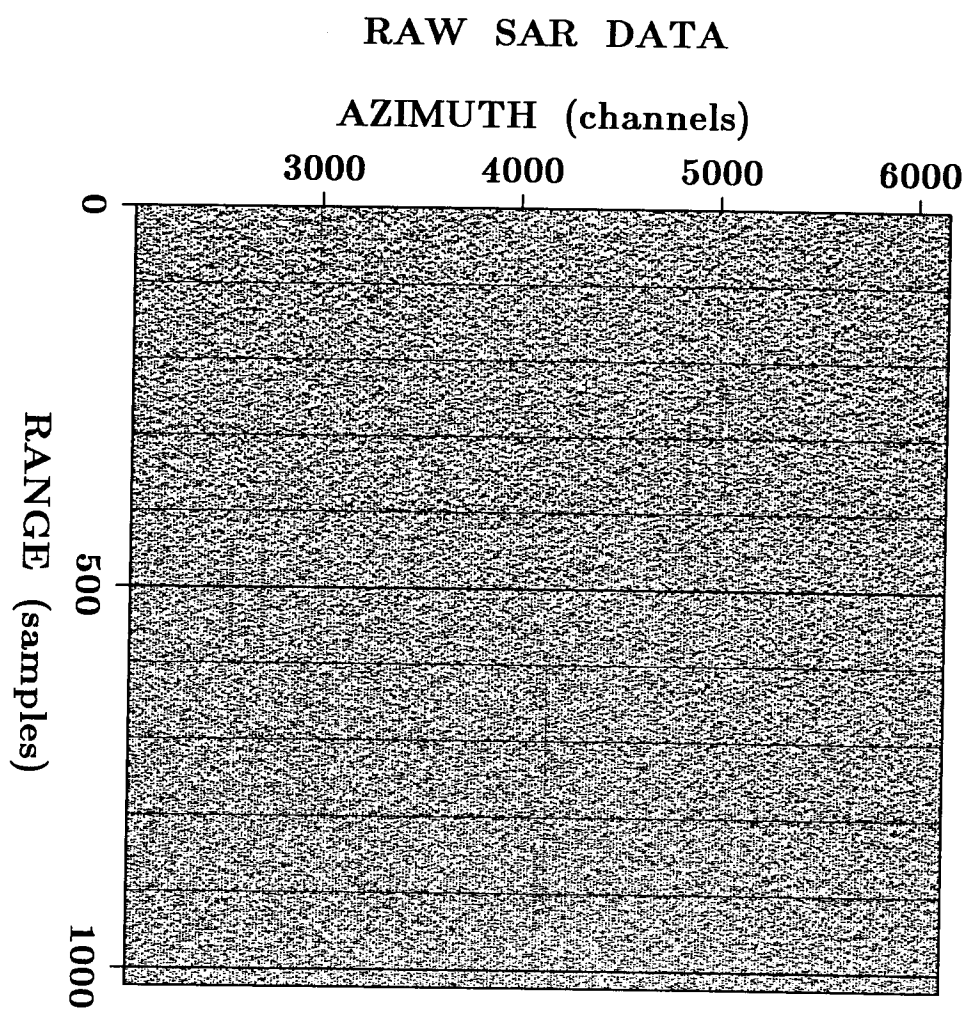

FIG. 2. Uncorrelated SAR data Only one out of sixteen channels used in this study shown. Channels 2048-6144 and samples 0-4096 used from 16384 channel x 13860 sample dataset.

Expanding the square root in equation (1) gives the phase shift used in for the data processing in this article:

$$e^{-i\frac{k_x^2 c^2}{8k_\tau}\tau_0}. \tag{3}$$

Figure 5 plots this phase shift. The source-receiver slant angle α (tilt of streaks in Figure 4) is corrected with the azimuthal wavenumber bias

$$k_x = k_x + \frac{\omega_0}{c}\sin(\alpha), \tag{4}$$

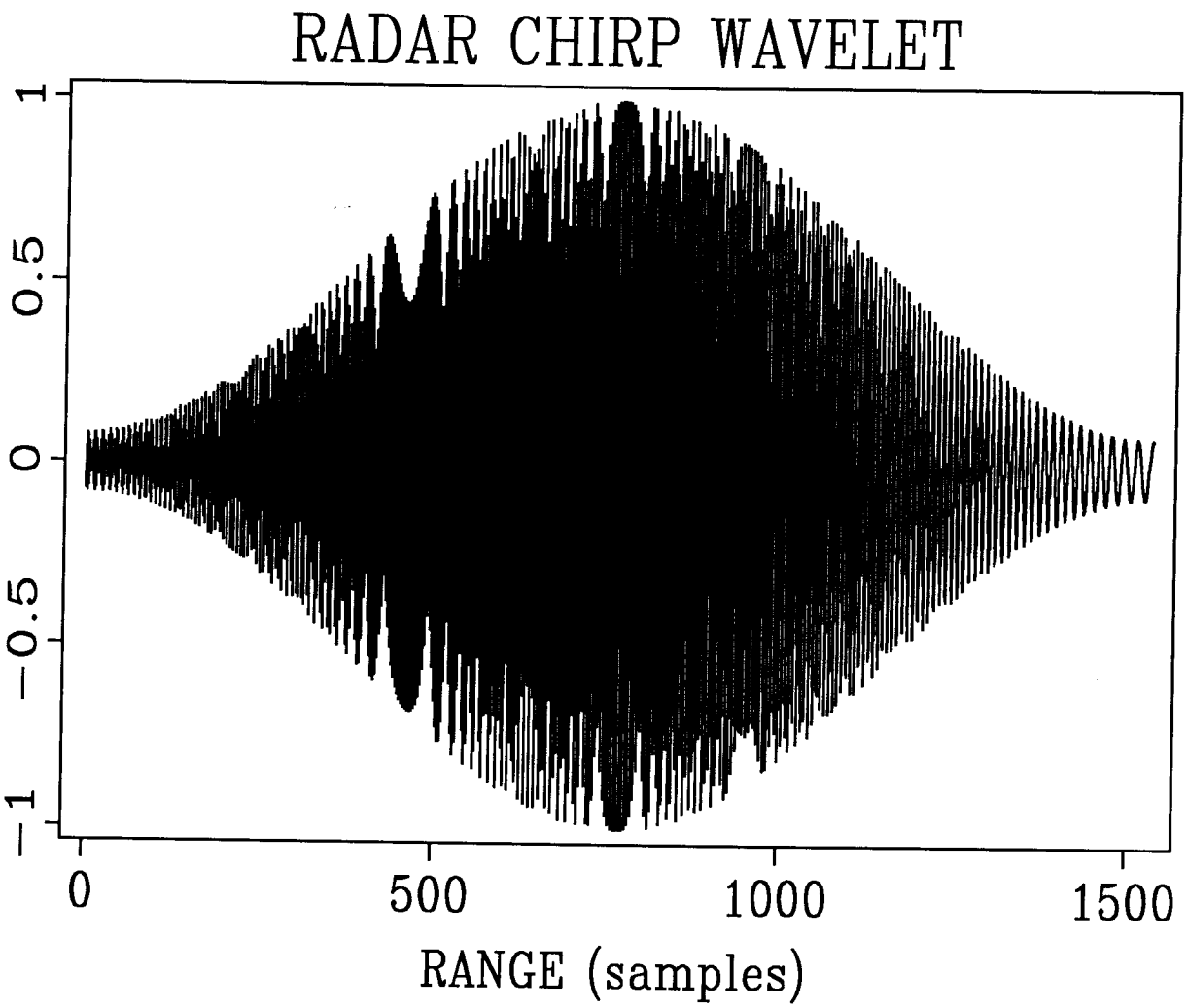

FIG. 3. Correlation radar chirp wavelet. Sampling is 45.53 MHz, low is 11.38 MHz, band is 19 MHz, and duration is 33.8 usec.

$$k_x = k_x + \frac{\omega_0}{c}\sin(\alpha), \tag{4}$$

where ω_0 is the center chirp frequency.

Some comments concerning implementation. First, the phase argument in equation (3) is very large, over a thousand radians instead of a couple in seismics. Double precision calculations and computing the exponential modulus 2π handles this. Second, the slant bias of equation (4) can exceed the k_x nyquist. This apparent aliasing can be removed by taking replacing k_x with its 2π modulus.

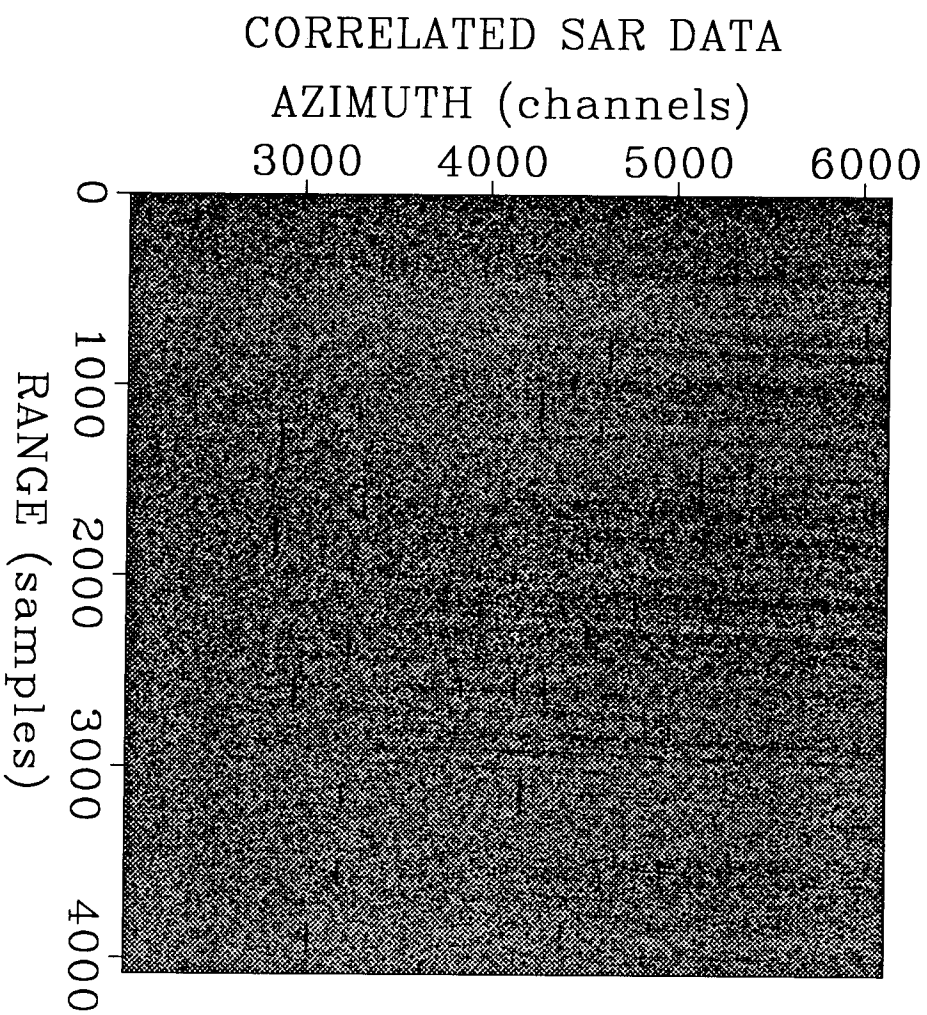

FIG. 4. Correlated SAR data. Same data subset as Figure 2. Streaks are analogous to seismic linear-moved-out diffractions. Diffraction aperture is several thousand channels.

Multilook and display

Inverse Fourier transforming over sub-ranges of azimuthal wavenumber (Figure 6) is equivalent to illuminating the image at different angles. Summing over several of these so-called "looks" (Figure 7) helps remove specular noise and fill in parts of images absent in a given look.

Since SAR data is in the specular regime (wavelength $<<$ CDP), the standard seismic display of wavefield phase appears random. Smoothed modulus of the complex SAR wavefield is displayed instead.

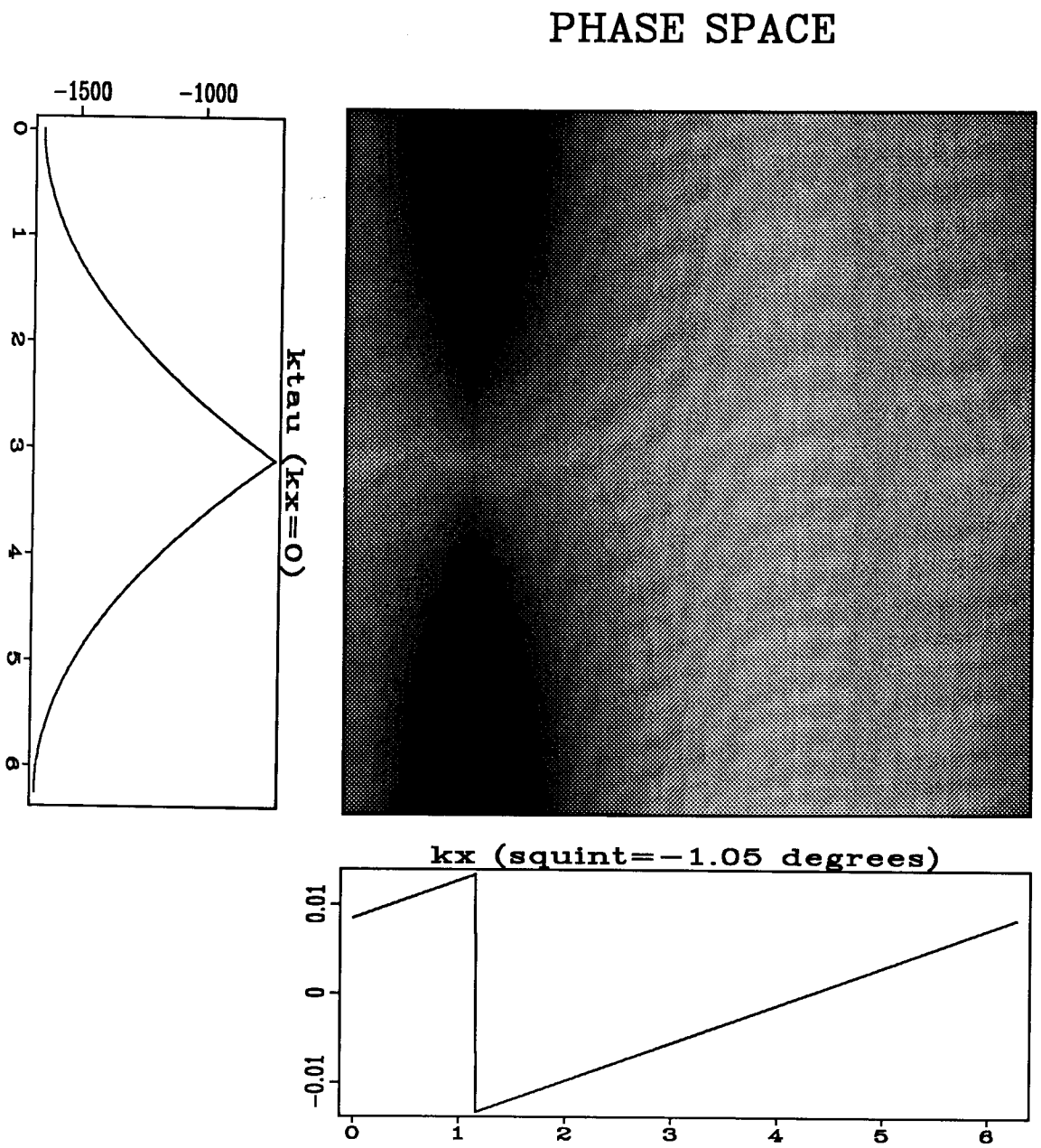

FIG. 5. Phase shift space and two cross-sections. Phase shifts of several thousand radians occur. The lateral displacement is the squint slant correction. The temporal frequency varies only two percent about the central wavelength.

COMPUTER IMPLEMENTATION

The huge size of SAR dataset— a quarter giga-samples per panel— brought back memories of doing Stolt migrations on a 64K core memory DEC PDP-11. Most of the processing stages of Figure 1 can be done on single channel vectors or data sub-panels. The pig-in-the-python is the forward cross-vector FFT which must be done out-of-core even on a 64MB Convex. The twelfth-portion data subset used in this study takes about 30 CPU minutes to fully process on a Convex.

Because of slant aliasing, decimating azimuthal channels does not work well. Instead, imaging swaths of a thousand or so channels is better. There is enough holographic-like redundancy across the long diffraction streaks (Figure 4) so that a reasonable image can be obtained from just a portion of the streak.

The SAR dataset also strained our display facilities. Interesting images may be several thousand pixels on side which exceeds the scrolling capabilities of graphics terminals or dithering resolution of laser printers. I was able to get the best display contrast by turning off the wiggle lines in a variable-area seismogram display.

Since the quarter giga-sample dataset is only about a half second of real time data, SAR data processing will continue to be a frontier in super-computing research.

FUTURE PLANS

This preliminary SAR imaging exercise mostly replicates the work of Rocca's Milan research group (Bonanomi, 1987). It's successful goal was to provide a departure point for future combined SAR-seismic imaging research. Among possible topics are fk-interpolation imaging methods, auto-focusing, higher-order imaging corrections, and more efficient computer implementation.

REFERENCES

Bonanomi, V. and Guzzi, M., 1987, Stolt migration generalized for electromagnetics in an array processor: E.E. Thesis, Milan Politechnic

Gazdag, J., 1978, Wave equation migration with the phase shift method: Geophysics, v.43, p.1342-1351

Rocca, F., 1987, Synthetic aperture radar: a new application for wave equation techniques: SEP-56

Stolt, R., 1978, Migration by Fourier transform: Geophysics, v.43, p.23-48

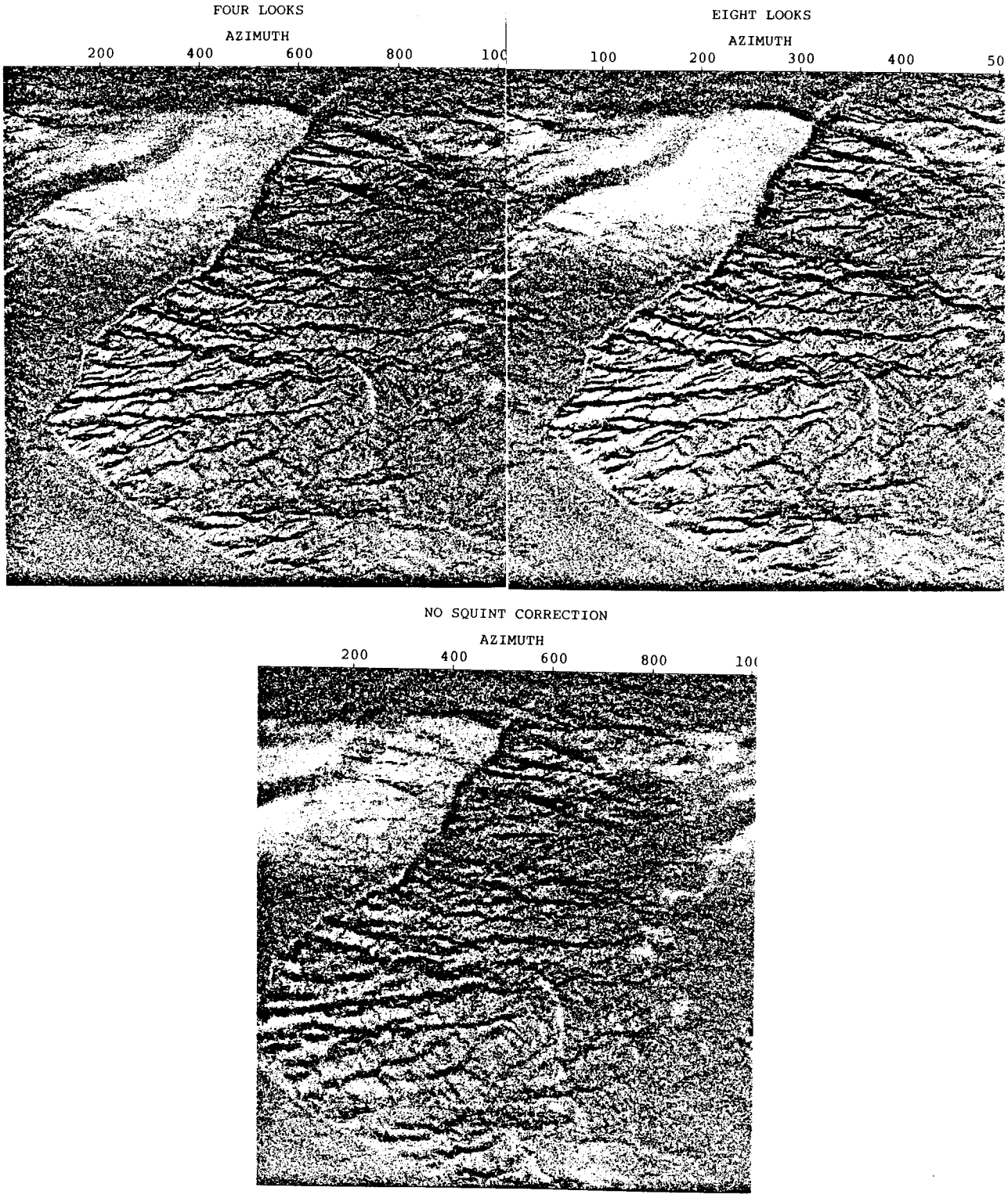

FIG. 7. Final images. All are multi-look sums to reduce speckle and increase coverage. Upper-left sums the four looks of Figure 6. Upper-right is an eight look sum. Below is imaging without the slant correction. The selection and orientation of looks is on-going research.

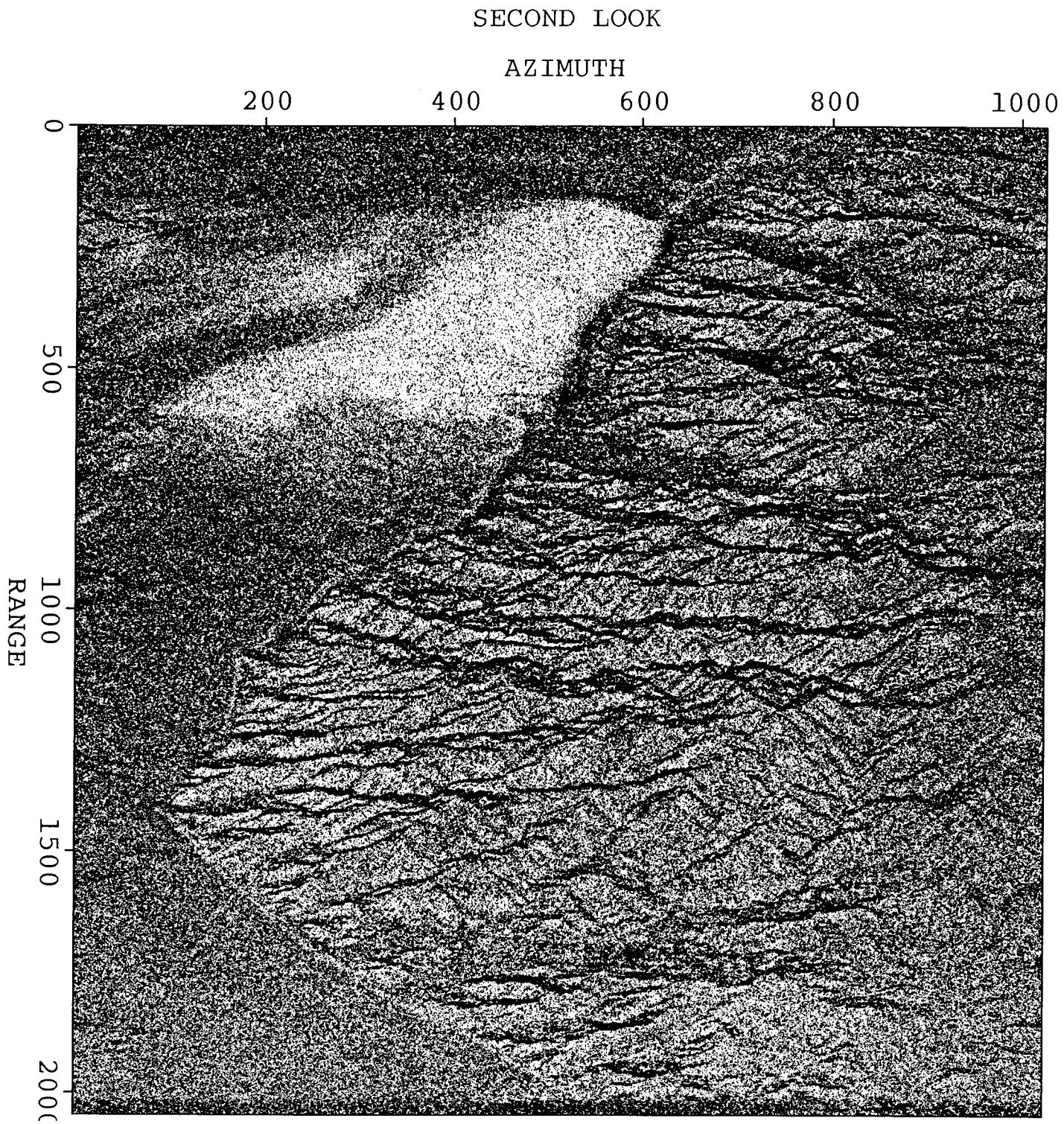

FIG. 6b. Expanded display of the upper-right look of Figure 6.

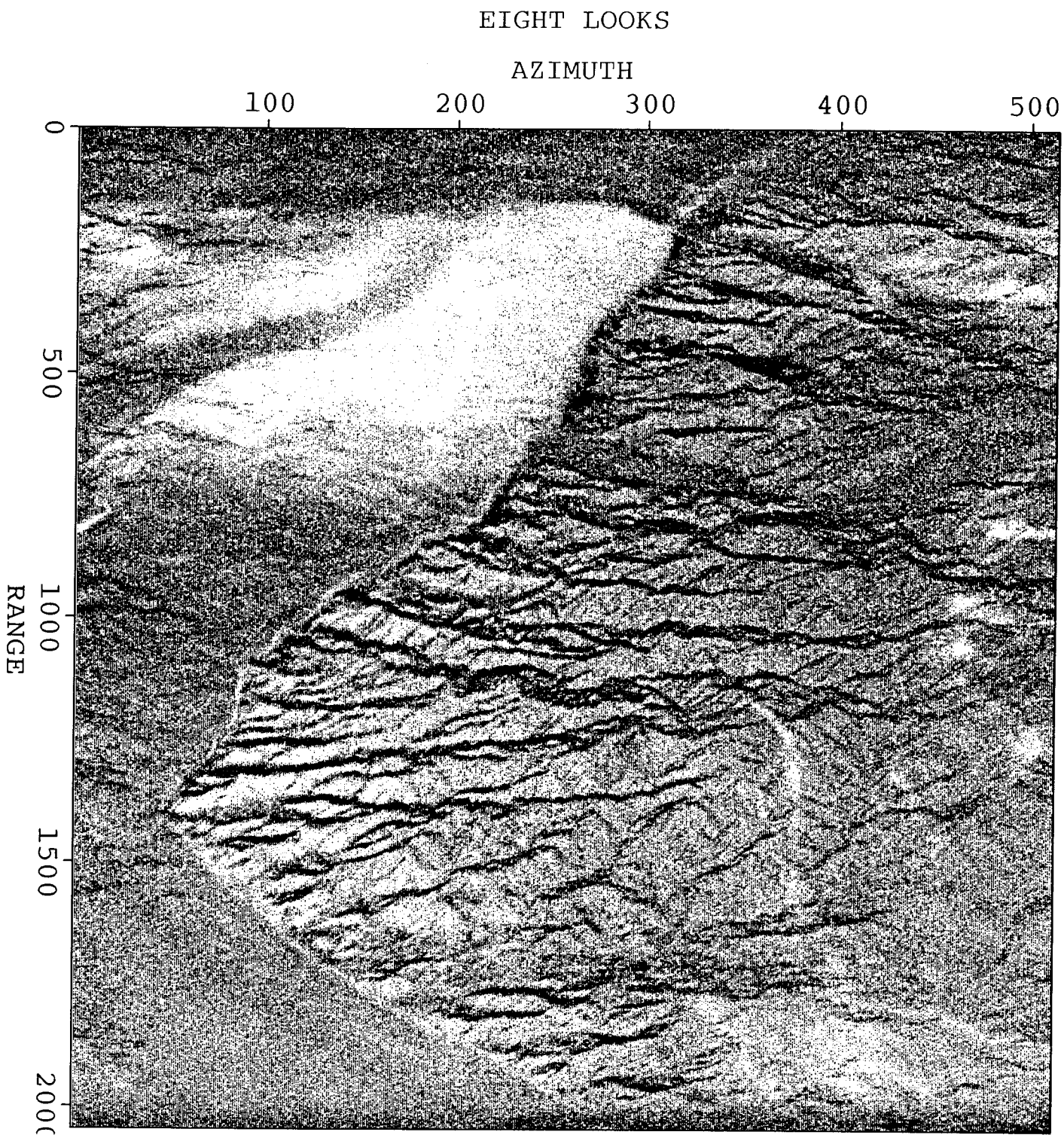

FIG. 7b. Expanded display of the eight look sum.